The International Conference on Technologies and Materials for Renewable Energy, Environment and Sustainability, TMREES14

Entropy Generation due to Viscous Dissipation around a Wells Turbine Blade: A Preliminary Numerical Study

Ahmed S. Shehata[a*], Khalid M. Saqr[b,] Mohamed Shehadeh [c], Q. Xiao [a], Day A.H.[a]

[a] Department of Naval Architecture, Ocean and Marine Engineering, University of Strathclyde, Glasgow G4 0LZ, U.K

[b] Mechanical Engineering Department, College of Engineering and Technology
Arab Academy for Science Technology and Maritime Transport, P.O. 1029 AbuQir, Alexandria, EGYPT

[c] Marine Engineering Department, College of Engineering and Technology
Arab Academy for Science Technology and Maritime Transport, P.O. 1029 AbuQir, Alexandria, EGYPT

Abstract

The present work analyzes, through a rigorous numerical investigation, the entropy generation due to viscous dissipation around a Wells turbine blade. Two-dimensional numerical models for four NACA airfoils were built and validated against experimental measurements under steady flow conditions. The models were used to assess the entropy generation for flows achieving 10° angle of attack. It was found that the entropy generation around the NACA0015 airfoil blade is less by approximately 12% than the entropy generation around NACA0012, NACA0020 and NACA0021 airfoils. Then, the NACA0015 and NACA0021 airfoils were simulated under different flow conditions (i.e. Reynolds number and angle of attack). The results were discussed in the light of Wells turbine performance objectives.

1.   INTRODUCTION

There have been several attempts to find methods to convert the mechanical energy of marine waves into useful work to produce electrical power. Oscillating water column (OWC) is one of such methods, where the wave

* Corresponding Author: Ahmed S. Shehata, *E-mail address:* ahmedsamir_marine@hotmail.com

 motion is used to drive oscillating air column. The main challenge of such method lies in finding an efficient technique to convert the linearly oscillating flow of air into a unidirectional rotary motion for driving an electrical generator .A novel solution of this problem is the Wells turbine (Wells 1976), in its standard design the air turbine rotor consists of several symmetrical airfoil blades positioned around a hub, the airfoils are based on the NACA [National Advisory Committee for Aeronautics] series. Because of its simple and efficient operation, The Wells turbine has already been applied in practice to gain energy from marine waves.

In the past two decades, experimental research of Wells turbine has mainly focused on improving the turbine performance with emphasis on the overall operational characteristics. The airfoils sections practically used in Wells turbine have been extensively investigated in aeronautical applications. However, the operating conditions in Wells turbine are completely different from such of the aeronautical applications. In Wells turbine, the rotor contains multiple blades, which are confined by a shroud aiming at harnessing the flow momentum to drive the rotor with the maximum torque. The flow physics in such situations are still having several issues to investigate, bearing in mind the dynamical complexity resulting from an OWC driven by random irregular marine waves.

The present work attempts to evaluate the entropy generation associated with viscous dissipation around different airfoils commonly considered in Wells turbine applications. The Gouy–Stodola theorem [1] postulates the difference between reversible and actual works in any thermodynamic system is the entropy generation in such system, as shown later in section 4. Such theorem is the foundation for the entropy generation minimization method proposed by Bejan to optimize finite size thermodynamic systems [2].

2.   LITERATURE REVIEW

The main idea behind the performance of Wells turbine is that it always rotates in the same direction, normal to the flow direction, although the air flow is oscillating. The manufacturing of Wells turbines is easier than for other turbines and they are able to work at low flow coefficients. Furthermore, OWC-based energy stations are considerably more compact than other comparable energy conversion systems. [3]

Nevertheless, Wells turbines show some drawbacks compared to alternative systems: low efficiency, poor self-starting characteristics, short operating range, high axial force coefficient and low tangential force coefficient. Therefore, many researchers have attempted to identify the optimum operating conditions to overcome such drawbacks and improve the performance of Wells turbines [4, 5]. This section briefly reviews the most relevant studies to accentuate the scope of the present work.

In a number of previous studies, it was concluded that the delay of stall onset contributes in improving Wells turbine performance. This delay can be achieved by setting guide vanes on the hub near the rotor[6]. It was found that the running and starting characteristics of the Wells turbine with 3D guide vanes are superior to those with 2D guide vanes or without guide vanes. In addition, the presence of end plates was investigated by [7, 8] where it was concluded that the Wells turbine with end plates is superior to those of the original Wells turbine (the peak efficiency and the stall margin increased by approximately 4%) and the characteristics are dependent on the size and position of end plate.

Three dimensional numerical simulations were performed by [9] in order to analyze the performance of a Wells turbine with CA9 blade profile, A maximum efficiency of 70% was obtained. Moreover, [10] have used numerical simulation to study the effect of the blade sweep on the performance of a Wells turbine using either NACA0020 or CA9 blade profiles. It was found that the performance of the Wells turbines with the NACA0020 and the CA9 blades was influenced by the blade sweep. As the optimum rotor shape for a NACA0020 blade, a blade sweep ratio 35% was identified to deliver the optimum performance. It was also found that the overall turbine performance for the NACA0020 is better than such of the CA9. In another study [11], the characteristics of a Wells turbine with NACA0021 constant chord blades were investigated. It is found from the numerical results in such study that the wakes behind the turbine blades merge rigorously in the portion of radius ratio from 0.45 to 1.0, which leads the turbine to stall.

Two-stage Wells turbines involving symmetric airfoils and Non-Symmetric airfoils have been investigated in [12, 13]. Systematic optimization procedure has been carried out to optimize the performance of the turbine as a function of the non-dimensional gap between the two rotors, leading to an optimal value of the non-dimensional gap near 0:85 when considering the operating range. Moreover, the Evolutionary Algorithms were used to estimate the optimum shape with an increase of efficiency (by 2.1%) and of tangential force coefficient (by 6%), compared to the standard NACA 2421 and for the one-stage the optimum shape with an increase of efficiency (by 1%) and of

tangential force coefficient (by 11.3%), compared to the standard NACA 0021. On the other hand, the hysteretic characteristics of monoplane and biplane have been studied by [14, 15]. The objective of such works was to investigate into the aerodynamic losses of the Wells turbine. It was found that for the biplane, the hysteretic behavior was similar to that of the monoplane at lower attack angles, but the hysteretic loop similar to the dynamic stall was observed at higher attack angles.

3. OBJECTIVE AND SCOPE

The objective of the present work was essentially to investigate the entropy generation, due to viscous dissipation, around Wells turbine airfoils in two-dimensional steady flow configurations. Two factors were tested; the flow Reynolds number and the airfoil angle of attack. The scope of work aims to highlight the effect of operating conditions on the second law analysis of Wells turbine. The computational work presented in this paper also demonstrates the performance of three turbulence models in the flow under investigation, and pinpoints the order of cells used in respective CFD models. The scope was limited to four airfoils namely NACA0012, NACA0015, NACA0020 and NACA0021. These airfoils are common to use in Wells turbine applications.

4. MATHMEATICAL MODEL AND NUMERICAL APPROACH

The mathematical model consists of the governing equations of turbulent incompressible steady flow in two-dimensional generalized coordinates, which can be written in vector notations as:

Continuity:
$$\frac{\partial}{\partial x_i}(\bar{u}_i) = 0 \tag{1}$$

RANS:
$$\frac{\partial}{\partial x_i}(\rho \bar{u}_i \bar{u}_j) = -\frac{\partial p}{\partial x_j} + \frac{\partial}{\partial x_j}\left[\mu\left(\frac{\partial \bar{u}_i}{\partial x_j} + \frac{\partial \bar{u}_j}{\partial x_i} - \frac{2}{3}\delta_{ij}\frac{\partial \bar{u}_j}{\partial x_i}\right)\right] + \frac{\partial}{\partial x_j}\left(-\overline{\rho u_i' u_j'}\right) \tag{2}$$

where $\bar{u}$ is the Reynolds averaged velocity vector, p is the pressure field, ρ is the density and μ is the molecular viscosity. The present study adopts one and two-equation turbulence models to close the Reynolds stress term $\left(-\overline{\rho u_i' u_j'}\right)$ of the RANS equation [16] as shown in the following section. The transport equations of such models can be found in turbulence modeling texts such as [17]. These equations are skipped here for brevity. The second law of thermodynamic defines the net-work transfer rate $\dot{W}$ as [18]:

$$\dot{W} = W_{rev} - T_o S_{gen} \tag{3}$$

where W_{rev} is the reversible work, S_{gen} is the total entropy generation rate and T_o is reservoir temperature. It is possible to express the irreversible entropy generation in terms of the derivatives of local flow quantities in the absence of phase changes and chemical reactions, the two dissipative mechanisms in viscous flow are the strain-originated dissipation and the thermal dissipation, which correspond to a viscous S_V and a thermal S_t entropy generation respectively [19]. Thus, we can write:

$$S_{gen} = S_V + S_{th} \tag{4}$$

In incompressible isothermal flow, such as the case in hand, the thermal dissipation term vanishes. The local viscous irreversibilities thereof can be expressed as:

$$S_V = \frac{\mu}{T_o}\phi \tag{5}$$

where ϕ is the viscous dissipation term, expressed in two dimensional Cartesian coordinates as:

$$\phi = 2\left[\left(\frac{\partial u}{\partial x}\right)^2 + \left(\frac{\partial v}{\partial y}\right)^2\right] + \left(\frac{\partial u}{\partial y} + \frac{\partial v}{\partial x}\right)^2 \tag{6}$$

and the global entropy generation is hence expressed as:

$$\bar{S} = \iint\limits_{xy} S_V \, dy dx \qquad (7)$$

4.1   NUMERICAL MODEL

The computational domain was discretized to Cartesian structured finite volume cells using GAMBIT code. Dirichlet boundary conditions were applied on the domain for the solution of momentum and continuity equations via specifying values of the incoming air velocity and the far field gauge pressure. The application of such boundary condition types matches the Green-Gauss cell based evaluation method for the gradient terms used in the solver (ANSYS FLUENT). Numerous tests accounting for different interpolation schemes used to compute cell face values of the flow field variables, as well as convergence criteria have been undertaken. It was found that the second order upwind interpolation scheme yields results that are approximately similar to such yielded by third order MUSCL scheme. It was also found that the solution reaches convergence when the scaled residuals approaches 1×10^{-6}. At such limit, the flow field variables holds constant values with the application of consecutive iterations.

4.2   MODEL TESTING AND VERIFICATION

In order to ensure that the numerical model is free from numerical diffusion and artificial viscosity errors, several grids were tested to estimate the number of grid cells required to establish a grid-independent solution. Table 1 shows the specifications of different grids used in such test. Figure 1 shows the pressure coefficient distribution on the upper and lower surfaces of the airfoil as computed by the four grids. Grid C was chosen to conduct the analysis presented hereafter.

Table 1 specification of grids

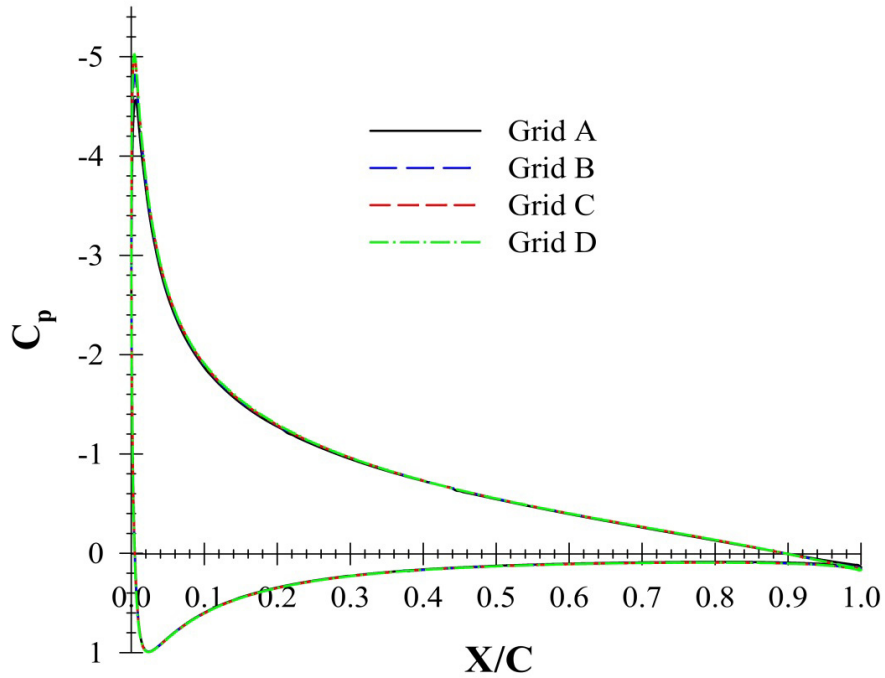| Grid	No. of Cells	first cell	Growth rate	Aspect ratio	EquiAngle skew
A	112603	1×10^{-4}	1.02	1.996	0.429
B	200017	1×10^{-5}	1.015	2.466	0.475
C	312951	1×10^{-5}	1.012	2.376	0.514
D	446889	1×10^{-6}	1.01	2.551	0.513

Figure 1. Pressure coefficient plotted on the normalized airfoil cord for different grid resolutions.

4.3   *VALIDATION AND TURBULENCE MODEL COMPARISON*

Three turbulence models were used to model the flow around NACA0020 airfoils in order to determine the model which gives the best agreement with experimental data adopted from [20]. All models performed quite well in the simulation yielding predictions which are in excellent agreement with measurements, as shown in figure2. The S-A model, however, showed slight underpredictions near to the blade leading edge in comparison with the other two models. The $k - \omega$ SST model required more time than the Realizable $k - \varepsilon$ model, yielding similar results. Therefore, the latter model was adopted in the following simulation cases.
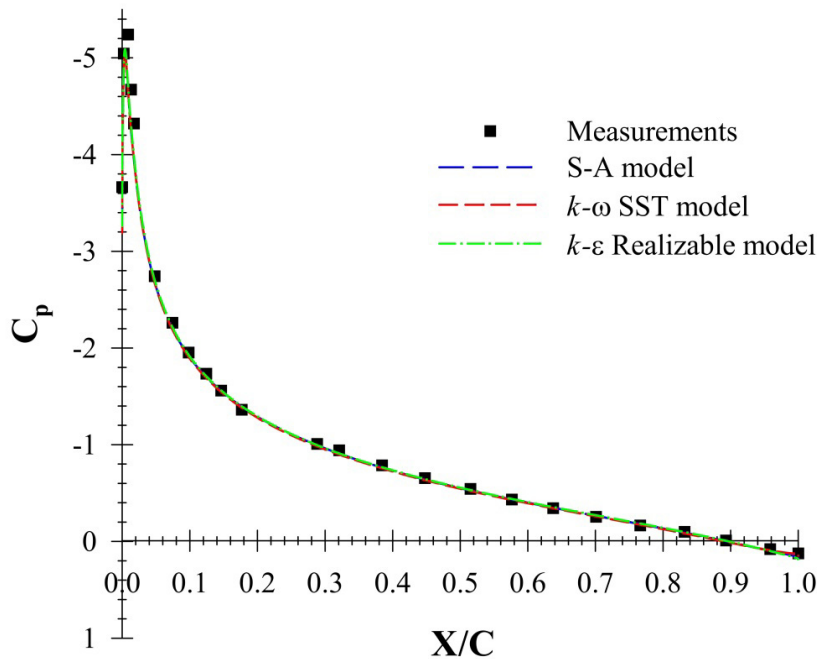
Figure 2. Pressure coefficients with the cord length of blade for different viscous model

5. RESULTS AND DISCUSSION

The numerical simulations were used to obtain local entropy viscosity predictions of the different airfoil sections. There is a wide dispute in literature on the optimum airfoil of the NASA standard sieries for Wells turbine applications. A considerable number of studies cite the results of [21] as a reference for considering NACA 0021 airfoil to give the optimum performance for conventional Wells turbines. However, as formerly mentioned there are numerous experimental and numerical studies, which have different and sometime contradicting, results mainly based on tangential force and first law efficiency. The present work aspires to shed the light on such dispute from another perspective; second-law analysis. Figure 3 shows a comparison between the total (i.e. integral) entropy generation for four different airfoils. The NACA0015 airfoil section gives less value of total entropy generation.

To study the relationship between the Reynolds number effect and the entropy, we simulated the flow over NACA0015 and NACA0021 airfoils under different Reynolds number, as shown in figure 6. The Reynolds number had radical effect on the entropy generation. When re was increased from 6×10^4 to 1×10^5 the total entropy generation increased correspondingly more than two folds for both airfoils. However, when Re was increased further to 2×10^5 the total entropy generation exhibited unintuitive values ranging from 25% less to 20% higher than the corresponding value at Re = 1×10^5 for both airfoils, as shown in figure 4. The reason behind such phenomena can be attributed to the nonlinear complexity of the viscous dissipation term (equation 6) where both the square of mean rate of strain and velocity divergence contributes to the local viscous irreversibilities. This phenomenon suggests that possible existence of critical Reynolds number at which viscous irreversibilities takes minimum values.
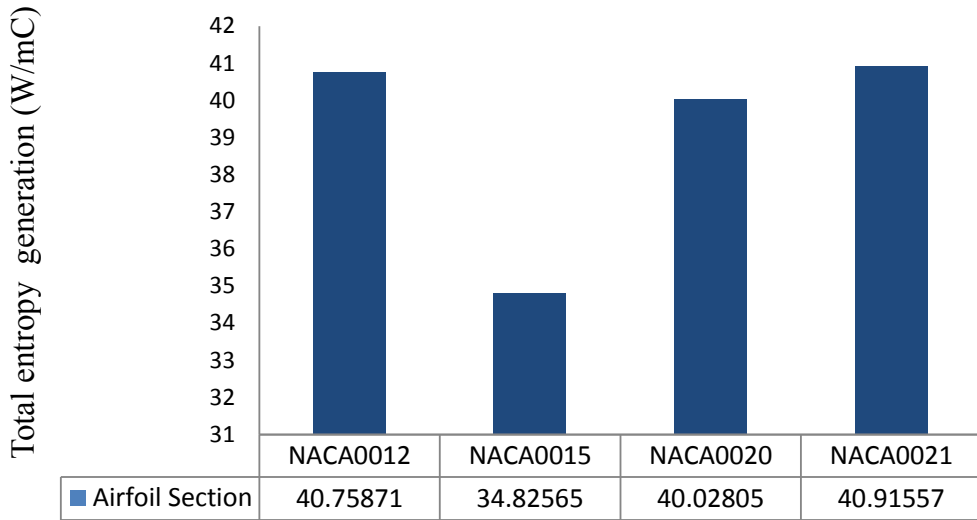
Total entropy generation (W/mC)	NACA0012	NACA0015	NACA0020	NACA0021
■ Airfoil Section	40.75871	34.82565	40.02805	40.91557

Figure 3 The Entropy-viscosity integral with different airfoil sections

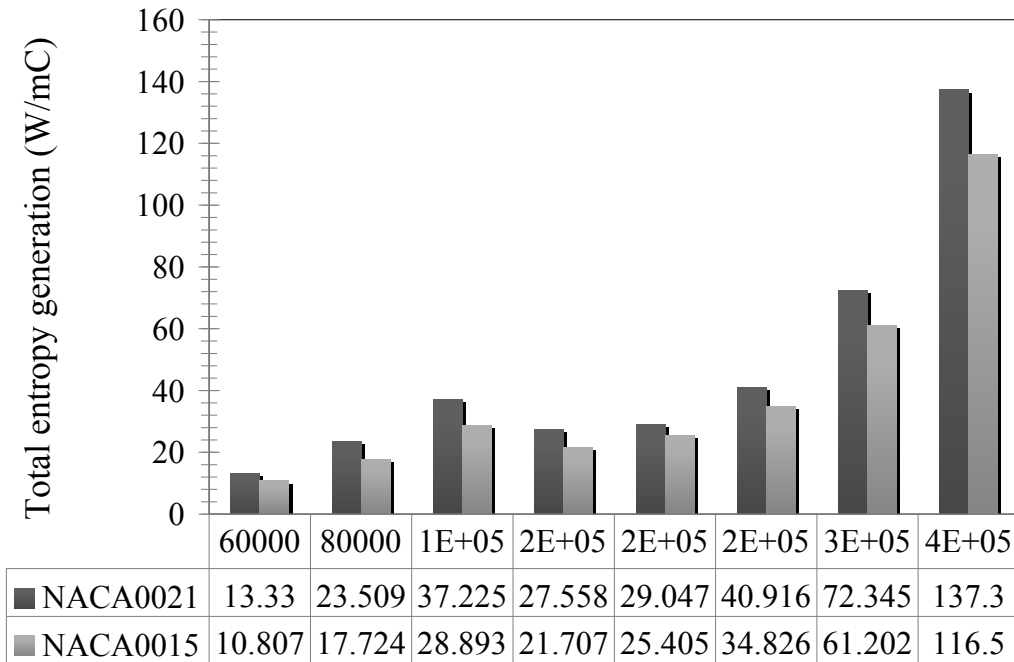| Total entropy generation (W/mC)	60000	80000	1E+05	2E+05	2E+05	2E+05	3E+05	4E+05
■ NACA0021	13.33	23.509	37.225	27.558	29.047	40.916	72.345	137.3
■ NACA0015	10.807	17.724	28.893	21.707	25.405	34.826	61.202	116.5

Figure 4. The Entropy-viscosity integral with different Reynolds Number

The increase of angle of attack had a direct effect to the total entropy generation in the flow over both airfoils, similar to the effect of Reynolds number. However, as shown in figure 5, each airfoil had a different entropy

generation signature for different angle of attack. NACA0021 airfoil yielded less entropy generation than NACA0015 at low angles ($\theta < 20^{\circ}$), while such trend was reversed when higher angles were considered.
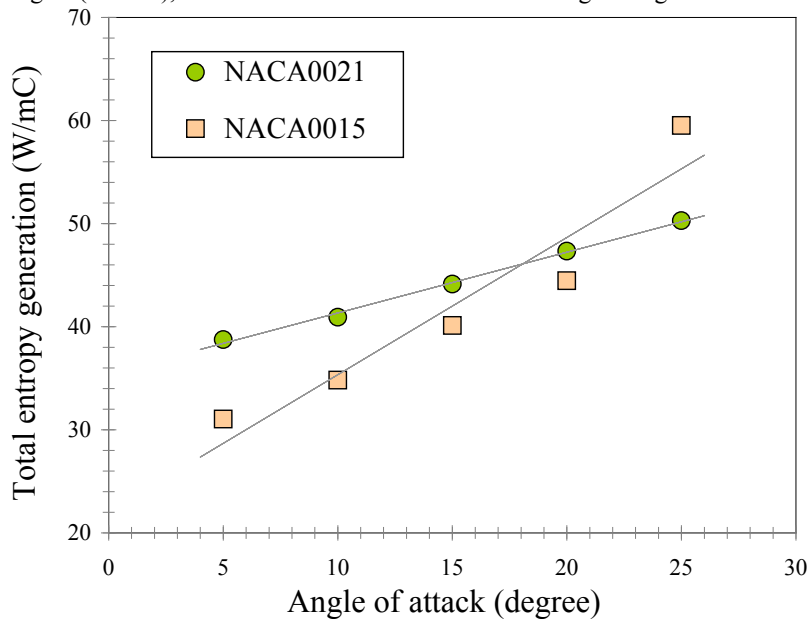
Figure 5. The Entropy-viscosity integral with different angle of attack

6.   CONCLUSION

Second law analysis of Wells turbine requires accurate estimation of flow irreversibilities around the turbine blades. This can be effectively done via accurate CFD models. Two-dimensional incompressible steady flow simulations of multiple airfoils revealed than the geometry as well as the operating conditions have radical effects on the total entropy generation in the flow around turbine airfoil. The results have evidently shown that the entropy generation is an optimization measure for improving the aerodynamics, hence overall performance, of Wells turbine. Future work will investigate the characteristics of entropy generation under unsteady and three-dimensional flows with a special emphasis on the viscous dissipation term and its production limits.

7.   REFERENCES

1.   Bejan, A., Entropy Generation Minimization: The Method of Thermodynamic Optimization of Finite-Size Systems and Finite-Time Processes. 1995: Taylor & Francis.
2.   Bejan, A., Entropy generation minimization: The new thermodynamics of finite-size devices and finite-time processes. Journal of Applied Physics, 1996. 79(3): p. 1191-1218.
3.   Cruz, J., OceanWave Energy. 2008: springer.
4.   Takao, M., Effect of Blade Profile on the Performance of Large-Scale Wells Turbine, in The Fourteenth International Offshore and Polar Engineering Conference. 2004, The International Society of Offshore and Polar Engineers: Toulon, France.
5.   Brito-Melo, A., Analysis of Wells turbine design parameters by numerical simulation of the OWC performance. Ocean Engineering, 2002. 29: p. 1463–1477.
6.   Setoguchi, T., Effect of guide vane shape on the performance of a Wells turbine. Renewable Energy, 2001. 23: p. 1-15.
7.   Mamun, M., IMPROVEMENT OF THE PERFORMANCE OF THE WELLS TURBINE BY USING A VERY THIN ELONGATED ENDPLATE AT THE BLADE TIP, in the 3rd BSME-ASME International Conference on Thermal Engineering. 2006, ASME: Dhaka, Bangladesh.
8.   Takao, M., et al., Wells turbine with end plates for wave energy conversion. Ocean Engineering, 2007. 34(11-12): p. 1790-1795.
9.   Thakker, A., Numerical Analysis of Wells Turbine Performance Using a 3D Navier Stokes Explicit Solver, in International Offshore and Polar Engineerbtg Conference. 2001: Stavanger, Norway.
10.   Kim, T.H., Numerical investigation on the effect of blade sweep on the performance of Wells turbine. Renewable Energy, 2002. 25: p. 235-248.
11.   Dhanasekaran, T.S. and M. Govardhan, Computational analysis of performance and flow investigation on wells turbine for wave

energy conversion. Renewable Energy, 2005. 30(14): p. 2129-2147.
12. Mohamed, M.H., PERFORMANCE OPTIMIZATION OF A MODIFIED WELLS TURBINE USING NON-SYMMETRIC AIRFOIL BLADES, in Turbo Expo 2008: Power for Land, Sea and Air GT. 2008, ASME: Berlin, Germany.
13. Mohamed, M.H., et al., Multi-objective optimization of the airfoil shape of Wells turbine used for wave energy conversion. Energy, 2011. 36(1): p. 438-446.
14. Kinoue, Y., et al., Hysteretic characteristics of monoplane and biplane Wells turbine for wave power conversion. Energy Conversion and Management, 2004. 45(9-10): p. 1617-1629.
15. Mamun, M., et al., Hysteretic flow characteristics of biplane Wells turbine. Ocean Engineering, 2004. 31(11-12): p. 1423-1435.
16. Wilcox, D.C., Turbulence Modeling for Computational Fluid Dynamics. 2006: DCW Industries, Incorporated.
17. Hirsch, C., Numerical Computation of Internal and External Flows: The Fundamentals of Computational Fluid Dynamics. 2007: Elsevier Science.
18. Bejan, A., Entropy generation minimization- The new thermodynamics of finite-size devices and finite-time processes. APPLIED PHYSICS REVIEWS, 1995.
19. Iandoli, C.L., 3-D Numerical Calculation of the Local Entropy Generation Rates in a Radial Compressor Stage. International journal of thermodynamics, 2005. 8: p. 83-94.
20. Gregory, N. and C. O'reilly, Low-speed aerodynamic characteristics of NACA 0012 aerofoil section, including the effects of upper-surface roughness simulating hoar frost. 1970: National Physical Laboratory Teddington, England.
21. Raghunathan, S., C. Tan, and N. Wells, Wind tunnel tests on airfoils in tandem cascade. AIAA Journal, 1981. 19(11): p. 1490-1492.